ACS ORGANIC & INORGANIC Au
AN OPEN ACCESS JOURNAL OF THE AMERICAN CHEMICAL SOCIETY

pubs.acs.org/orginorgau

Article

Predictability of Chalcogen-Bond-Driven Crystal Engineering: An X-ray Diffraction and Selenium-77 Solid-State NMR Investigation of Benzylic Selenocyanate Cocrystals

Vijith Kumar, Michael Triglav, Vincent M. Morin, and David L. Bryce*

Cite This: ACS Org. Inorg. Au 2022, 2, 252–260

Read Online

ACCESS | Metrics & More | Article Recommendations | Supporting Information

ABSTRACT: We describe a series of new chalcogen-bonded cocrystals featuring 1,2-bis(selenocyanatomethyl)benzene (**DSN**) and 1,2,4,5-tetrakis(selenocyanatomethyl)-benzene (**TSN**) as the donor moieties and a variety of Lewis bases such as onium halides, *N*-oxides, and pyridine-containing heterocycles as the acceptors. Single-crystal X-ray diffraction demonstrates that, in every case, the selenocyanates consistently interact with the acceptor molecules through strong and directional Se···X chalcogen-bonds (ChBs) (X = halides, oxygen, and nitrogen). ^{77}Se solid-state nuclear magnetic resonance spectroscopy was applied to measure selenium chemical shift tensor magnitudes and to explore potential correlations between these tensor elements and the local ChB geometry. In every case, the isotropic ^{77}Se chemical shift decreases, and the chemical shift tensor span increases upon cocrystallization of **DSN** with the various ChB acceptors. This work contributes to a growing body of knowledge concerning the predictability and robustness of chalcogen bonds in crystal engineering as well as the NMR response to the establishment of chalcogen bonds. In particular, among the systems studied here, highly linear chalcogen bonds are formed exclusively at the stronger σ-hole of each and every selenium atom regardless of the size, charge, or denticity of the electron donor moiety.

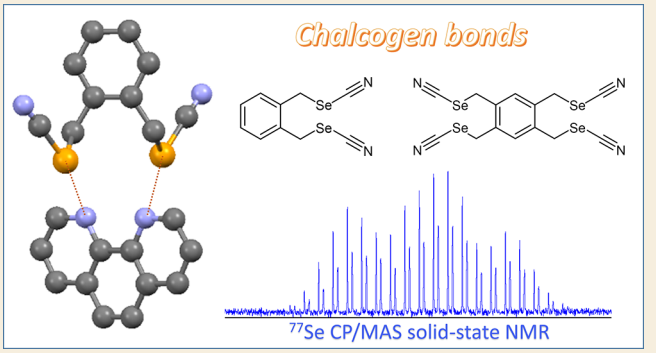

KEYWORDS: *crystal engineering, noncovalent interactions, chalcogen bonds, NMR spectroscopy*

INTRODUCTION

Crystal engineering concerns the control of solid-state molecular organization with the understanding of intermolecular interactions such as strength and directionality to ultimately realize desirable functional outcomes.[1] Hydrogen bonding (HB) has been the most ubiquitous and expansively investigated noncovalent interaction for several decades.[2] Following the marked development of the arena of halogen bonding (XB) over the last 20 years or so,[3] it is now well-established that elements of groups 14, 15, 16, and 18 of the periodic table are similarly apt to possess electrophilic sites (σ-holes)[4] and to form attractive interactions[5] with Lewis bases giving rise to tetrel,[6] pnictogen,[7] chalcogen,[8−11] and aerogen bonds, respectively.[12] A very recent study reported on the direct experimental measurement and visualization of σ-holes via Kelvin probe force microscopy.[13]

The chalcogen bond (ChB), in analogy with the halogen bond,[14] has been defined by IUPAC as a "net attractive interaction between an electrophilic region associated with a chalcogen atom in a molecular entity and a nucleophilic region in another, or the same, molecular entity".[15] The strength of the ChB interaction increases with the polarizability of the donor atom[16] as described by their static scalar dipole polarizabilities: S = 19.4 au, Se = 28.9 au, and Te = 38.0 au (a.u. = atomic units). Additionally, electron-withdrawing groups increase the Lewis acidity of the chalcogen donor site and consequently the interaction strength.[17] Due to its directionality and strength, the chalcogen bond has a notable potential for application in several fields of chemistry, biochemistry, and materials science. Several applications have been reported over the years[10] in various fields such as supramolecular chemistry,[8,18,19] protein and peptide structure,[20,21] crystal engineering,[22−24] anion recognition and transport,[25,26] chemical synthesis and organocatalysis,[27,28] and pharmaceutical chemistry.[29,30]

In contrast to halogen atoms that are well-known to develop a single localized area of depleted electron density and elevated electrostatic potential (σ-hole) along the prolongation of the

Received: November 12, 2021
Revised: January 26, 2022
Accepted: January 26, 2022
Published: February 9, 2022

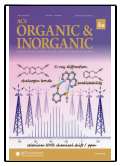

https://doi.org/10.1021/acsorginorgau.1c00051
ACS Org. Inorg. Au 2022, 2, 252−260

C—X bond,[31] chalcogen atoms can provide two σ-holes, characteristically roughly along the extensions of the C−Ch covalent bonds.[25,32] Theoretical work on model compounds by Politzer et al.[33] and experimentally determined X-ray crystal structures of $Se(CN)_2$ and $Te(CN)_2$ from Klapotke et al.[34,35] show that there are deviations between the location of the maximum ($V_{s,max}$) of the electrostatic surface potential (ESP), the extension of the C−Ch bond axis, and the Ch···X axis (X = ChB acceptor). Such deviations, along with the existence of two σ-holes, render the predictability of ChB interactions more challenging, and the uses of these interactions based on the tenets of crystal engineering are somewhat limited. A number of crystal structures of amphoteric chalcogen-bonded molecules are known, wherein a molecule behaves as both the ChB donor and acceptor, such as dicyanoselenide,[34] dicyanotelluride,[35] benzoselenadiazoles,[18] selenophthalic anhydrides,[32] telluradiazoles,[36] and iso-tellurazole *N*-oxides.[37] There are also several instances of heteromeric systems designed purely based on chalcogen bonds; for example, dicyanotelluradiazole and dicyanoselenadiazole cocrystallized with anions;[38] benzotelluradiazole derivatives and thiophenes as anionic receptors;[39,40] thiophene, selenophene, and tellurophene receptors for anion recognition;[41] intermolecular ChB with chalcogenadiazoles and in pure iso-tellurazole *N*-oxides;[18,42] chalcogenazolo-pyridine scaffolds;[43] and considerable work from Fourmigué and co-workers on organic selenocyanate derivatives as strong, directional chalcogen bond donors with utility in crystal engineering applications.[23,44−47]

Solid-state characterization is key to understanding the physicochemical properties of solid materials, as intermolecular interactions can have significant impacts on these properties. Single-crystal X-ray diffraction (SCXRD) is a commonly used experimental tool to examine the nature of ChB in the solid state. The use of complementary techniques such as solid-state nuclear magnetic resonance (SSNMR) provides additional information for crystalline systems and may be the best option for disordered materials. ^{77}Se (spin-1/2) possesses favorable NMR properties including a moderate natural abundance (7.63%) and gyromagnetic ratio ($\gamma = 5.12 \times 10^7$ rad T^{-1} s^{-1}). The chemical shift range of ^{77}Se spans over 3000 ppm.[48] Previously, we carried out a systematic study of double ChB between dicyanoselenodiazole and dicyanotelluradiazole with various Lewis bases with a combination of X-ray diffraction, SSNMR, and computational chemistry.[22,24] Motivated by the work of Fourmigué and co-workers,[23,44−47] we have also previously described the role of substituted benzylic selenocyanate derivatives for anion recognition and for crystal engineering with pyridyl moieties.[25,49]

Herein, we report the preparation of a series of cocrystals controlled by chalcogen bonds between substituted benzylic selenocyanates and a group of Lewis bases comprising halides, *N*-oxides, and pyridyl heterocycles (Figure 1). One objective of this study is to assess the predictability and robustness of ChB formation for a range of acceptor molecules with variable size, denticity, and charge. Cocrystals were characterized by SCXRD (8 out of 10 new cocrystals), powder X-ray diffraction (PXRD), and solid-state nuclear magnetic resonance spectroscopy. In addition, FTIR spectroscopy was also utilized as a tool for the rapid investigation of ChB in the cocrystals. This study explores systematic crystal engineering based on ChB and employs different solid-state characterization methods to provide experimental insights into possible relationships between NMR observables and the formation of chalcogen bonds in solids.

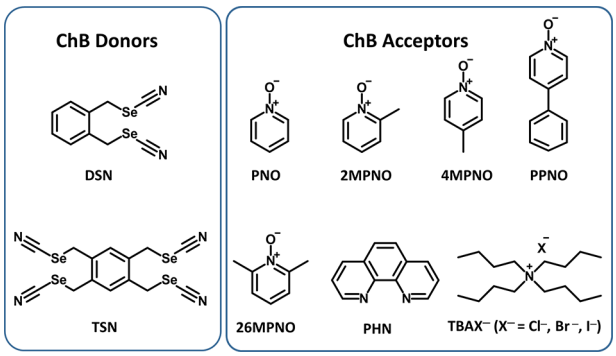

Figure 1. Molecular structures of the chalcogen bond donors (left) and acceptor molecules (right) in this work.

RESULTS AND DISCUSSION

Single-Crystal X-ray Diffraction and Structural Descriptions

ChB donors **DSN** and **TSN** were synthesized according to previous literature.[50,51] The solid-state structures of the donors have been previously reported by Fourmigué and co-workers, and these motifs crystallize thanks to the formation of infinite chains supported via intermolecular Se···NC chalcogen bonds.[23,44] The ChB formation is exemplified by 10 new cocrystals obtained by slow solvent evaporation, typically from acetone. Cocrystal formation is preliminarily confirmed by powder X-ray diffraction (PXRD) analysis (*vide infra*; see also Supporting Information (SI)) and measurements of the melting points of the cocrystals compared to those of the pure individual components. Single crystals of suitable quality for X-ray diffraction were obtained from slow evaporation at room temperature from a diethyl ether−acetone solution containing a ChB donor and a ChB acceptor as shown in Figure 1. Further experimental details and crystallographic information are provided in Tables S1 to S8 (SI). Crystals were held at 200 ± 2 K prior to data collection unless otherwise noted (SI). Structural characteristics of the chalcogen-bonded cocrystals such as Ch···X bond distances ($d_{Ch\cdots X}$), C−Ch···X bond angles ($\theta_{C-Ch\cdots X}$), and normalized contact parameters (N_c) are given in Table 1. The value of N_c is calculated as the quotient obtained by dividing the ChB distance by the sum of the van der Waals/Pauling radii of the donor and acceptor atoms (see Table 1).

The results are collected and discussed below according to the nature of the ChB acceptor, i.e., halides, *N*-oxides, and nitrogen-containing heterocycles.

Oxygen and Nitrogen Atoms as ChB Acceptors. *N*-oxides are widely used as molecular building blocks in crystal engineering, particularly as hydrogen and halogen bonding acceptor groups.[52] The availability of three electron pairs on the *N*-oxide oxygen enables monodentate, bidentate, and tridentate coordination and facile tunability of the acceptor properties as well as the opportunity for substitution on aromatic heterocycles. Our previous study described the formation of double chalcogen bonds between seleno/telluro imidazoles and various methyl-, methoxy-, and phenyl-substituted *N*-oxides.[24] Here, we cocrystallize benzylic selenocyanates with various substituted *N*-oxides to examine the robustness and predictability of ChB-driven self-assembly.

https://doi.org/10.1021/acsorginorgau.1c00051
ACS Org. Inorg. Au 2022, 2, 252−260

Table 1. C−Se···X Chalcogen Bond Geometries Determined with Single-Crystal X-ray Diffraction

compound	interaction	$d_{Ch\cdots X}$ (Å)	$\theta_{C-Ch\cdots X}$ (deg)	N_c	ref code
DSN·2MPNO	Se···O^-	3.025(3)	166.3(2)	0.91	this work
	Se···O^-	2.955(1)	168.1(1)	0.89	
DSN·26MPNO	Se···O^-	2.854(2)	169.6(3)	0.86	this work
DSN·PPNO	Se···O^-	2.961(1)	163.2(5)	0.89	this work
	Se···O^-	2.846(1)	168.7(5)	0.86	
DSN·PHN	Se···N	3.250(2)	158.8(9)	0.93	this work
DSN·TBACl	Se···Cl^-	3.100(2)	176.3(2)	0.85	this work
	Se···Cl^-	3.304(1)	170.3(2)	0.91	
DSN·TBABr	Se···Br^-	3.349(6)	169.6(2)	0.88	this work
	Se···Br^-	3.354(6)	176.1(1)	0.89	
DSN·TBAI	Se···I^-	3.528(1)	177.6(3)	0.88	this work
	Se···I^-	3.554(1)	177.5(3)	0.89	
	Se···I^-	3.532(1)	178.6(3)	0.89	
	Se···I^-	3.481(1)	177.3(4)	0.87	
TSN·TBACl	Se···Cl^-	3.304(2)	170.9(2)	0.88	SIZSOM
	Se···Cl^-	3.100(2)	174.7(3)	0.88	
	Se···Cl^-	3.176(2)	173.8(2)	0.87	
	Se···Cl^-	3.162(2)	171.1(2)	0.87	
TSN·TBABr	Se···Br^-	3.590(4)	176.9(1)	0.95	this work
	Se···Br^-	3.310(2)	171.0(1)	0.87	
	Se···Br^-	3.574(2)	171.1(1)	0.95	
	Se···Br^-	3.429(2)	179.3(1)	0.91	
TSN·TBAI	Se···I^-	3.451(9)	171.9(1)	0.87	GIHCUY
	Se···I^-	3.511(9)	170.8(1)	0.88	

Three of five acceptor−donor groupings produced single crystals of suitable quality for analysis with single-crystal X-ray diffraction, i.e., **DSN·2MPNO**, **DSN·26MPNO**, and **DSN·PPNO**, while **DSN·PNO** and **DSN·4MPNO** were obtained only as powders. Cocrystal **DSN·2MPNO** crystallizes in a triclinic system, space group *P*-1, with one molecule in a general position in the unit cell. As seen in Figure 2,

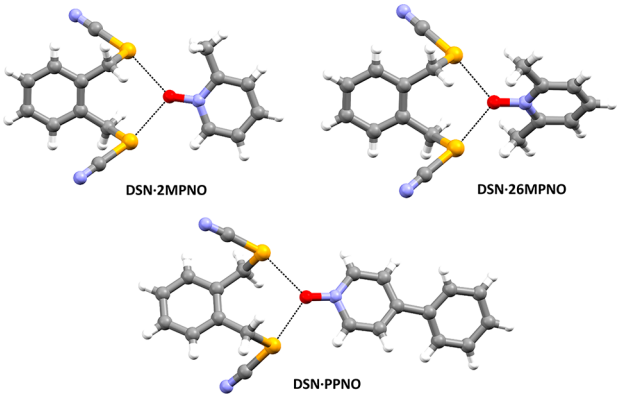

Figure 2. Ball and stick representations (Mercury 4.10.3) of chalcogen-bonded cocrystals **DSN·2MPNO**, **DSN·26MPNO**, and **DSN·PPNO.** Color code: gray, carbon; blue, nitrogen; white, hydrogen; yellow, selenium; red, oxygen (dashed black lines denote ChBs).

cocrystallization is mainly driven by strong N−Se···O^- chalcogen bonds between the donor and the *N*-oxide unit (N_c values of 0.89 and 0.91). ChBs are formed along the extension of the depleted electron density regions of the Se−N covalent bonds. The presence of two comparable ChB distances in **DSN·2MPNO** is consistent with the presence of a glide plane passing nearly through the center of the oxygen atom and collinear with the long axis of the **2MPNO** molecule. Moreover, the N−Se···O^- ChB angles are nearly 180°, concomitant with the strong and predictable directionality of such interactions. The **2MPNO** molecule is subject to positional disorder; modeling and structure refinement are described in the SI (section S.5). The oxygen atom in **2MPNO** interacts with the two different selenium sites of the selenocyanate. One ChB is shorter and more linear compared to the other; the longer interaction is due to the steric hindrance produced by methyl substitution (see Table 1). The ChBs are further stabilized by weak hydrogen bonds between the oxygen atom of **2MPNO** and the alkyl hydrogens of the benzylic selenocyanate.

Similarly, SCXRD analysis reveals that cocrystals of **DSN·26MPNO** and **DSN·PPNO** crystallize in monoclinic *C*2/*c* and orthorhombic *Fdd*2 space groups, respectively. **DSN·26MPNO** contains half a molecule of donor and acceptor in the asymmetric unit, while **DSN·PPNO** contains a single molecule on a general position in the unit cell. In all cases, the *N*-oxide molecule behaves as a bidentate ChB acceptor and interacts with two different selenium atoms. The ChBs are shorter, with N_c values of 0.86 and 0.89. Once again, the observed N−Se···O^- angles are close to 180° (169.6 and 163.2°, respectively), indicating the linearity of the interactions. Even with several trials, we were unable to obtain single crystals of **DSN·PNO** and **DSN·4MPNO** suitable for single-crystal X-ray diffraction. However, cocrystal formation is fully confirmed by PXRD and SSNMR spectroscopy (SI).

The ability of **DSN** to form supramolecular assemblies via chalcogen bonds was further assessed using various nitrogen-containing monotopic and ditopic heterocycles as ChB acceptors. Interestingly, we were able to isolate only one cocrystal, i.e., with 1,10-phenanthroline (**PHN**). **PHN** is a well-known ditopic electron donor. The yellow needles of **DSN·PHN** crystallize in a monoclinic system and the C2/*c* space

https://doi.org/10.1021/acsorginorgau.1c00051
ACS Org. Inorg. Au 2022, 2, 252−260

group. The asymmetric unit contains half a molecule each of **DSN** and **PHN**. ChBs between the preorganized chelating nitrogens and the Se sites of **DSN** are the driving force of the cocrystal formation (N_c = 0.93 and the N−Se···N angle is 158.8°). In **DSN·PHN**, Se acts as a ditopic donor (Figure 3a).

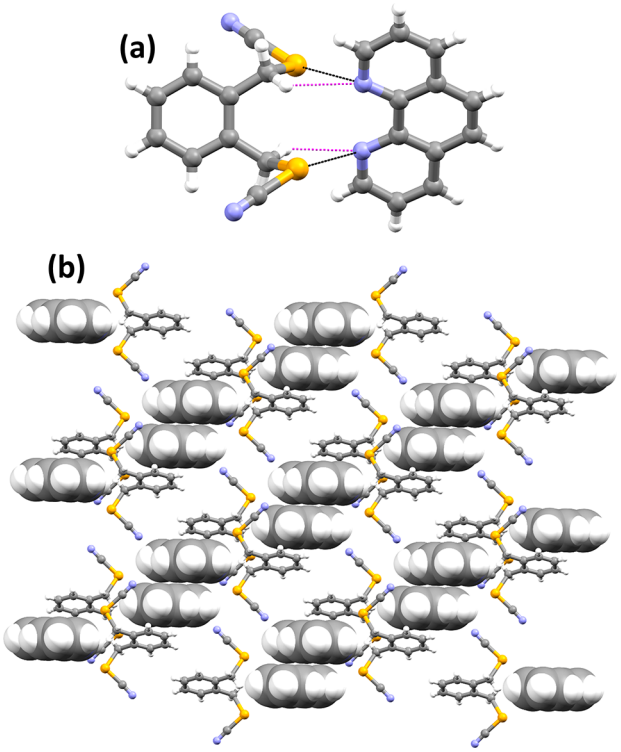

Figure 3. Ball and stick representations (Mercury 4.10.3) of the chalcogen-bonded cocrystal **DSN·PHN** (a). Crystal packing shows the formation of infinite chains (b).

One of the interactions is the ChB discussed above and the other is a weak hydrogen bond between the Se atom and an aromatic hydrogen atom of **PHN** (C−H···Se 3.097 Å). In addition, C−H···N hydrogen bonds (2.563 Å) also play a role in stabilizing the cocrystal structure. Moreover, C−H···π interactions in the **DSN** molecules create infinite chains, and the **PHN** molecules are sandwiched between these layers (Figure 3b).

Halide Anions as ChB Acceptors. We further cocrystallized **DSN** and **TSN** with tetrabutylammonium halides. Building on the reports from Fourmigué, this work is carried out to evaluate the predictability of ChB formation with anions, to examine the resulting structural features, and to probe these interactions using SSNMR spectroscopy. Three new salt cocrystals with **DSN** and with **TSN** were successfully synthesized, and single crystals were isolated. **DSN·TBACl** crystallizes in an orthorhombic system with the *Pbca* space group. The asymmetric unit contains a single molecule of each of **DSN** and **TBACl**. The Cl^- anion is μ_2-coordinated, i.e., every Cl^- anion is surrounded by two selenium atoms. The Cl^- anions interact with two Se sites of the selenocyanates along the prolongation of the covalent C−Se bonds. As described in Figure 4, two SeCN groups form noncovalent bonds with the Cl^- anion via short and directional chalcogen bonds (N_c of 0.85 and 0.91, N≡C−Se···Cl^- angles of 170.32 and 176.34°, respectively; see Table 1). In addition to the ChBs, C−H···Cl^- hydrogen bonds help to stabilize the crystal packing and contribute to the formation of continuous infinite chains.

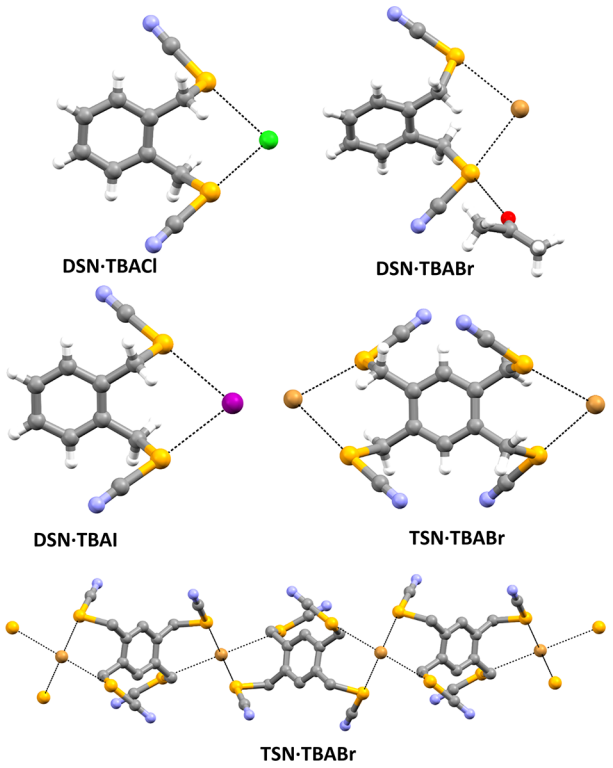

Figure 4. Ball and stick representations (Mercury 4.10.3) of chalcogen-bonded cocrystals **DSN·TBACl**, **DSN·TBABr**, **DSN·TBAI**, and **TSN·TBABr**. The μ_4 coordination geometry is shown in cocrystal **TSN·TBABr** (bottom).

Likewise, **DSN·TBABr** shows μ_2-bromide coordination, where each Br^- anion is surrounded by two selenium atoms. However, it crystallizes in a monoclinic system with the $P2_1/c$ space group. The asymmetric unit consists of a single unit of the salt cocrystal. **DSN·TBABr** also contains acetone solvent with an **DSN**/**TBABr**/acetone stoichiometric ratio of 1:1:1. The acetone molecule is positionally disordered over two sites. Structure solution and refinement of disorder details are described in the SI (section S.5). Similar to the **TBACl** cocrystal, the Br^- anions interact with two Se sites of the selenocyanates. As expected, the ChBs are short and directional, with N_c values of 0.88 and 0.89 and N≡C−Se···Br^- angles of 169.61 and 176.09°, respectively, (see Table 1). One of the Se atoms in **DSN** behaves as a ditopic ChB donor, participating in a Se···Br^- ChB and a Se···O ChB (Se···O distance 3.172 Å) with the disordered acetone. However, the C−Se···O angle of 147.93° is less linear compared to the N≡C−Se···Br^- angle (169.91°) due to the stronger σ-holes opposite the electron-withdrawing cyano group and the μ_2-bromide coordination. Further, we attempted to cocrystallize ChB donors with a heavier halide salt, namely tetrabutylammonium iodide. **DSN·TBAI** crystallizes in a monoclinic crystal system with the $P2_1/c$ space group and contains two molecules of **DSN** and two molecules of **TBAI**. Some terminal alkyl chains of the **TBAI** molecules show positional disorder and distorted thermal ellipsoids; refinement details are provided in the SI (section S.5). In total, there are four Se atoms and two I^- anions present in the asymmetric unit, and similar to **DSN·TBACl**, **DSN·TBAI** also undergoes μ_2-coordination, i.e., every I^- anion is surrounded by two selenium atoms. Similar to the

https://doi.org/10.1021/acsorginorgau.1c00051
ACS Org. Inorg. Au 2022, 2, 252−260

Table 2. Experimental ^{77}Se Chemical Shift Tensor Magnitudes[a]

compound	δ_{iso} (ppm)	Ω (ppm)	κ	δ_{11} (ppm)	δ_{22} (ppm)	δ_{33} (ppm)
DSN	326.1 (0.2)	629 (3)	0.45 (0.02)	593 (6)	420 (4)	−35 (4)
DSN·2MPNO	311.8 (0.1)	676 (2)	0.08 (0.007)	640 (2)	330 (2)	−36 (2)
DSN·26MPNO	322.3 (0.2)	674 (2)	0.01 (0.007)	658 (3)	325 (3)	−16 (2)
DSN·PPNO	311.9 (0.2)	680 (2)	0.06 (0.007)	645 (2)	326 (2)	−35 (2)
DSN·4MPNO	304.6 (0.02) (site 1)	694 (1)	0.09 (0.006)	640 (2)	327 (1)	−53 (2)
	297.0 (0.02) (site 2)	697 (2)	0.028 (0.007)	642 (2)	303 (2)	−54 (2)
DSN·PHN	319.8 (0.1)	689 (3)	0.069 (0.002)	656 (4)	335 (3)	−33 (2)
DSN·TBACl	303.2 (0.2) (site 1)	675 (5)	−0.040 (0.002)	646 (7)	293 (5)	−29 (5)
	289.9 (0.2) (site 2)	654 (4)	−0.069 (0.002)	624 (6)	275(4)	−29 (4)
DSN·TBABr	308.8 (0.3) (site 1)	671 (3)	−0.04 (0.002)	649 (6)	299 (4)	−21 (5)
	293.4 (0.3) (site 2)	667 (4)	0.03 (0.002)	623 (7)	300 (5)	−43 (5)
DSN·TBAI	311.8 (0.3) (site 1)	675(3)	0.007 (0.002)	639 (6)	313 (4)	−17 (5)
	309.2 (0.2) (site 2)	671 (3)	−0.007 (0.002)	645 (6)	307 (4)	−25 (5)
	302.8 (0.2) (site 3)	657 (3)	0.015 (0.020)	630 (6)	306 (4)	−28 (4)
TSN·TBABr	321.2 (0.2) (site 1)	733 (2)	−0.03 (0.004)	691 (5)	314 (5)	−41 (3)
	291.9 (0.3) (site 2)	688 (2)	0.12 (0.04)	622 (3)	320 (3)	−67 (4)
	271.7 (0.3) (site 3)	715 (2)	0.10 (0.006)	617 (4)	296 (3)	−98 (5)
	265.7 (0.2) (site 4)	708 (2)	0.077 (0.002)	611 (7)	284 (6)	−97 (5)

[a] $\delta_{iso} = (1/3)(\delta_{11} + \delta_{22} + \delta_{33})$; $\Omega = \delta_{11} - \delta_{33}$; $\kappa = 3(\delta_{22} - \delta_{iso})/\Omega$.

other cocrystals, each I^- anion interacts with two Se sites of the selenocyanates. Once again, the observed ChBs are short, with N≡C−Se···I^- distances of 3.481 to 3.554 Å (N_c ranges from 0.87 to 0.89). The N≡C−Se···I^- angles vary from 177.3 to 178°, consistent with the directionality of the interactions.

Cocrystal **TSN·TBABr** crystallizes in a monoclinic crystal system and the *C*2/*c* space group, and contains one molecule each of **TSN** and **TBABr** in the asymmetric unit. In **TSN·TBABr**, the Br^- anions sit on twofold axes and are μ_4-coordinated, i.e., every Br^- anion is surrounded by four selenium atoms, and this results in continuous chains (Figure 4, bottom). As expected, Se···Br^- interactions are chiefly responsible for the self-assembly of the cocrystal. Each bromide anion forms ChBs with four different selenium sites, and N≡C−Se···Br^- distances range from 3.310 to 3.590 Å (N_c = 0.87 to 0.95). The N≡C−Se···Br^- angles vary from 171.0 to 179.39°, demonstrating the linearity of the interactions. It is well-recognized that different halide anions can influence the preferential formation of different topologies in halogen-bonded systems,[53] due to different sizes, shapes, and coordination spheres of halides that can template different self-assembled structures correspondingly.[54] Our previous reports demonstrate the same tendency with the chalcogen bonds as a driving force in seleno/telluradiazoles; the results obtained here with benzylic selenocyanates demonstrate a similar propensity to template the various self-assembled structures.[22,25]

^{77}Se Solid-State NMR Spectroscopy and Powder X-ray Diffraction

To further understand the chemical and electronic structure associated with the chalcogen bonds in these systems, selenium-77 cross-polarization magic-angle spinning (CP/MAS) SSNMR experiments were carried out (Table 2; Figure 5; SI). Prior to these experiments, powder X-ray diffraction was used to determine whether the bulk powders were largely composed of crystallites consistent with the structures obtained from single-crystal X-ray diffraction. For cocrystals **DSN·2MPNO**, **DSN·PPNO**, and **DSN·TBACl**, good quality matches between experimental and simulated diffractograms were obtained (see SI). In the cases of **DSN·PHN**, **DSN·TBAI**, **TSN·TBABr**, and **DSN·26MPNO**, impurity peaks were noted in the diffractograms. Nevertheless, for these latter four samples, the ^{77}Se SSNMR spectra obtained were consistent with pure material and representative of the number of unique resonances expected from the SCXRD structures. We thus include these samples in our analyses of ^{77}Se chemical shift tensors. **DSN·TBABr** produced a PXRD pattern inconsistent with the SCXRD structure and yet produced a clean ^{77}Se SSNMR spectrum consistent with another polymorph (or anhydrate). Further included are ^{77}Se NMR data for **DSN·**

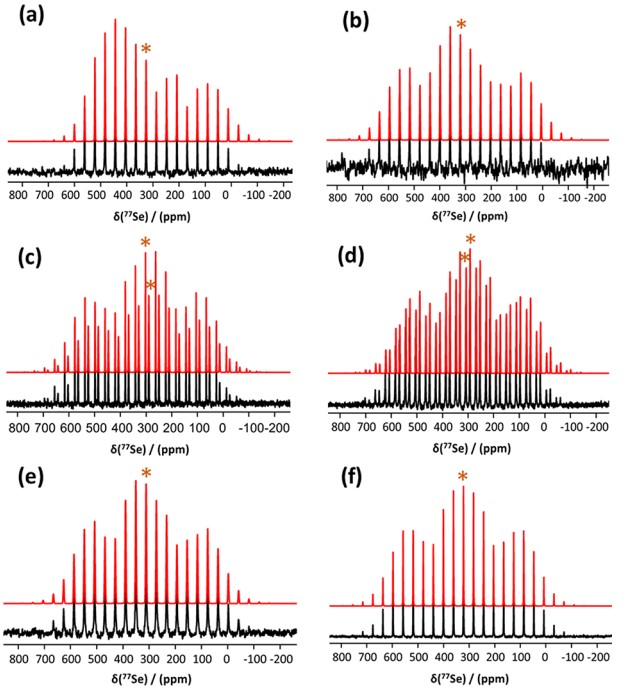

Figure 5. Examples of experimental ^{77}Se CP/MAS NMR spectra (black; B_0 = 9.4 T) for chalcogen-bonded systems and corresponding simulated spectra (red): (a) ChB donor **DSN**; (b) **DSN·PHN**; (c) **DSN·TBACl**; (d) **DSN·TBABr**; (e) **DSN·PPNO**; and (f) **DSN·26MPNO**. Asterisks indicate the isotropic chemical shifts.

https://doi.org/10.1021/acsorginorgau.1c00051
ACS Org. Inorg. Au 2022, 2, 252−260

4MPNO. Although a single-crystal X-ray diffraction structure was not obtained for this cocrystal, a well-resolved ^{77}Se CP/MAS NMR spectrum strongly suggests the presence of two crystallographically distinct sites, and the chemical shift data were thus included in Table 2. For powders featuring significant impurities or other ambiguous features in their ^{77}Se SSNMR spectra, it was not possible to rigorously determine chemical shift tensor data, and thus, these are excluded from Table 2.

Shown in Figure 5 are the ^{77}Se SSNMR spectra of **DSN** and several of its cocrystals, i.e., **DSN·PHN**, **DSN·TBACl**, **DSN·TBABr**, **DSN·PPNO**, and **DSN·26MPNO**. ^{77}Se SSNMR spectra of additional cocrystals are provided in the SI. The ^{77}Se CP/MAS SSNMR spectra were acquired at more than one MAS rate to distinguish the isotropic centerband from spinning sidebands. Acquiring data at more than one MAS rate also helps to increase the precision of the reported NMR parameters. A Herzfeld-Berger approach was used to analyze the spinning sideband manifolds and to determine the principal components of the selenium chemical shift tensor (δ_{11}, δ_{22}, δ_{33}). This approach assumes a negligible contribution from ^{77}Se−^{14}N residual dipolar coupling.

The ^{77}Se NMR spectrum of **DSN** reveals a single isotropic chemical shift at 326.1 ppm. The SCXRD structure shows two crystallographically distinct selenium sites; however, these are apparently too similar to resolve via ^{77}Se chemical shifts.

Investigation of the ^{77}Se chemical shift tensor data in Table 2 shows that there are significant changes upon chalcogen-bonded cocrystal formation. Cocrystal formation is associated with an increase in the value of the largest principal component, δ_{11}, relative to that for **DSN**. This is true for oxygen-, nitrogen-, and halide-based electron donors. The value of δ_{11} for the cocrystals of **DSN** varies from 623 to 658 ppm compared to the starting material at 593 ppm. Similarly, the value of the intermediate component (δ_{22}) decreases in the chalcogen-bonded cocrystals relative to pure **DSN**. For example, the value of δ_{22} of the cocrystals of **DSN** ranges from 275 to 335 ppm compared to the starting material at 420 ppm. These changes result in a decreased isotropic ^{77}Se chemical shift and increased CS tensor span upon cocrystal formation. The isotropic chemical shifts, δ_{iso}, of the cocrystals of **DSN** range from 293.4 to 322.3 ppm compared to pure **DSN** at 326.1 ppm. The value of the span, Ω, for the **DSN** cocrystals ranges from 654 to 697 ppm compared to the starting material at 629 ppm.

In halogen-bonded systems, it is well-studied that smaller contact distances and more highly linear geometries are associated with stronger interactions. Assessment of the ^{77}Se chemical shift tensor values as a function of the ChB geometry obtained from SCXRD revealed no strong correlations with the ChB length or angle. The lack of such correlations implies that additional structural features such as crystal packing and other weak interactions also influence the chemical shift tensor.

Intermolecular interactions including hydrogen bonds and halogen bonds affect IR band intensity variations and changes in spectral frequency.[55,56] In our previous work, we employed FTIR and Raman spectroscopies to detect the occurrence of chalcogen bonds.[49] All cocrystals obtained here with **DSN** were characterized by FTIR spectroscopy. C−Se stretching vibrations fall in the spectral region of approximately 500 cm^{-1}; due to overlap with the noise, it is difficult to confidently measure such peaks. However, the NC−Se vibration band of **DSN**, which appears at 2145 cm^{-1}, was red-shifted for the cocrystals to values between 2140 and 2143 cm^{-1}. This small reduction in vibrational wavenumber is consistent with previous related work[49] and could be used to assess the formation of chalcogen bonds in an indirect manner.

CONCLUSIONS

New chalcogen-bonded cocrystals of benzylic selenocyanates with various Lewis bases have been prepared and analyzed using spectroscopic and diffraction-based methods.

In all cocrystals, each and every selenium atom interacts via a single σ-hole, which coincides with the extension of the NC−Se covalent bond. Cocrystal formation has been observed with negatively charged and neutral Lewis bases to form isolated systems or extended supramolecular structures. The structures obtained here demonstrate the ability to chelate the Lewis bases via NC−Se···X interactions: isolated packing in the case of phenanthroline, *N*-oxide derivatives and μ_2 or μ_4 coordination in the case of halide acceptors. Furthermore, chalcogen bond formation occurs exclusively only at the strongest σ-hole site on each selenium atom and not at the weaker one. The work demonstrates the robustness of chalcogen-driven self-assembly with respect to a substantial array of electron donors.

^{77}Se CP/MAS SSNMR experiments reveal clear changes in the selenium chemical shift tensor principal components upon formation of chalcogen bonds. Decreases in the isotropic chemical shift and in the intermediate principal component (δ_{22}) in all cocrystals relative to the ChB donor **DSN** are observed. Increases in the span and in the largest principal component (δ_{11}) for the cocrystals in comparison with a pure ChB donor are also observed. Unfortunately, none of the ^{77}Se chemical shift tensor components correlate well with the local ChB geometry. The lack of this correlation implies that other structural features such as crystal packing and hydrogen bonding likely influence their values. Nevertheless, the qualitative changes in the selenium chemical shift tensor upon cocrystal formation are clearly associated with the formation of chalcogen bonds. In addition, IR spectroscopic investigation demonstrates that the NC−Se vibration band is also sensitive to chalcogen bonding, decreasing by a few wavenumbers in the cocrystals relative to the band seen for pure **DSN**.

In summary, this work contributes to a growing body of literature on crystal engineering using chalcogen bonds, in particular providing several new examples demonstrating the robust predictability of this interaction for the design of new materials.

EXPERIMENTAL SECTION

Preparation of Cocrystals

ChB donors **DSN** and **TSN**[23,44,50,51] and acceptors such as tetrabutyl ammonium halides, **PHN**, and *N*-oxides were dissolved separately in acetone (detailed synthetic procedure is provided in the SI (section S.3). These two solutions were mixed and allowed to evaporate slowly at room temperature to obtain the cocrystals.

Powder X-ray Diffraction

Pure ChB donors, ChB acceptors, and cocrystals were individually packed in an aluminum or glass sample holder, and data sets were collected on a Rigaku Ultima IV powder diffractometer at 293 K (±2) (Cu Kα_1 radiation with a wavelength of λ = 1.54056 Å). The measurements were carried out in focused beam geometry with a step-scan technique in a 2θ range of 5−50°. Data were acquired by scintillation counter detector in continuous scanning mode with a

https://doi.org/10.1021/acsorginorgau.1c00051
ACS Org. Inorg. Au 2022, 2, 252−260

step size of 0.02°. Experimental PXRD patterns and simulated patterns from the single crystal are provided in the SI.

Single-Crystal X-ray Diffraction

Single crystals were mounted on MiTeGen MicroMounts prior to data collection. Crystals were cooled to 200 ± 2 K prior data collection (unless mentioned in the SI, Tables S1 to S8). The data were collected on a Bruker AXS diffractometer equipped with Mo Kα radiation (wavelength of λ = 0.7103 Å) with an APEX II CCD detector. The raw data collection and processing were performed with the Bruker APEX II software package. Structure solution and refinement details are provided in the SI (Section S.5, Tables S1−S8).

Solid-State NMR Spectroscopy

All NMR experiments were conducted using a Bruker Avance III NMR spectrometer (B_0 = 9.4 T, ν_L (^{77}Se) = 76.311 MHz) and a triple-resonance 4 mm MAS NMR probe. Samples were gently ground into fine powders and packed in 4 mm o.d. zirconium oxide rotors prior to data collection. ^{77}Se SSNMR chemical shifts were referenced to solid $(NH_4)_2SeO_4$, (δ_{iso} = 1040.2 ppm). The MAS frequency was varied from 3.0 to 12.5 kHz to obtain spectra with a sufficient number of sidebands for spectral fitting purposes (SI). Spectra were generally obtained at 298 K; in a few cases, the temperature was set to 288 or 278 K due to the low melting point of some of the cocrystals. A standard ^{1}H → ^{77}Se cross-polarization (CP) pulse sequence with proton decoupling was employed. The $\pi/2$ pulse length was optimized to be 3.2 μs, and the CP contact time used was 7000 μs. The recycle delay varied from 10 s to 4 min. The total number of transients varied 512 from to 16000. The ^{77}Se NMR spectra were simulated using a Herzfeld-Berger analysis[57] and dmfit.[58] Selenium-77 SSNMR spectra for the pure ChB donors and the chalcogen-bonded cocrystals not shown in Figure 5 are provided in the SI.

■ ASSOCIATED CONTENT

Supporting Information

The Supporting Information is available free of charge at https://pubs.acs.org/doi/10.1021/acsorginorgau.1c00051.

Synthetic details, X-ray diffraction refinement details and data tables, powder X-ray diffractograms, ^{77}Se solid-state NMR spectra (PDF)

Accession Codes

CCDC 2117906 and 2117908−2117914 contain the supplementary crystallographic data for this paper. These data can be obtained free of charge via www.ccdc.cam.ac.uk/data_request/cif, or by emailing data_request@ccdc.cam.ac.uk, or by contacting The Cambridge Crystallographic Data Centre, 12 Union Road, Cambridge CB2 1EZ, UK; fax: +44 1223 336033.

■ AUTHOR INFORMATION

Corresponding Author

David L. Bryce − *Department of Chemistry and Biomolecular Sciences, University of Ottawa, Ottawa, Ontario K1N 6N5, Canada;* orcid.org/0000-0001-9989-796X; Phone: +1-613-562-5800; Email: dbryce@uottawa.ca; Fax: +1-613-562-5170

Authors

Vijith Kumar − *Department of Chemistry and Biomolecular Sciences, University of Ottawa, Ottawa, Ontario K1N 6N5, Canada;* Present Address: AbbVie, Ballisodare, County Sligo, Ireland. (V.K.)

Michael Triglav − *Department of Chemistry and Biomolecular Sciences, University of Ottawa, Ottawa, Ontario K1N 6N5, Canada;* orcid.org/0000-0002-9154-7612

Vincent M. Morin − *Department of Chemistry and Biomolecular Sciences, University of Ottawa, Ottawa, Ontario K1N 6N5, Canada*

Complete contact information is available at: https://pubs.acs.org/10.1021/acsorginorgau.1c00051

Notes

The authors declare no competing financial interest.

■ ACKNOWLEDGMENTS

Dedicated to Professor T. N. Guru Row on the occasion of his 70th birthday. D.L.B. is grateful to the Natural Sciences and Engineering Research Council of Canada for funding.

■ REFERENCES

(1) Desiraju, G. R. *Crystal Engineering: The Design of Organic Solids*; Elsevier: Amsterdam, 1989.

(2) Desiraju, G. R.; Steiner, T. *The Weak Hydrogen Bond in Structural Chemistry and Biology*; International Union of Crystallography monographs on crystallography; Oxford University Press, 1999.

(3) Cavallo, G.; Metrangolo, P.; Milani, R.; Pilati, T.; Priimagi, A.; Resnati, G.; Terraneo, G. The Halogen Bond. *Chem. Rev.* **2016**, *116*, 2478−2601.

(4) Cavallo, G.; Metrangolo, P.; Pilati, T.; Resnati, G.; Terraneo, G. Naming Interactions from the Electrophilic Site. *Cryst. Growth Des.* **2014**, *14*, 2697−2702.

(5) Alcock, N. W. Secondary Bonding to Nonmetallic Elements. *Adv. Inorg. Chem. Radiochem.* **1972**, *15*, 1−58.

(6) Bauzá, A.; Mooibroek, T. J.; Frontera, A. Tetrel-Bonding Interaction: Rediscovered Supramolecular Force? *Angew. Chem., Int. Ed.* **2013**, *52*, 12317−12321.

(7) Moaven, S.; Andrews, M. C.; Polaske, T. J.; Karl, B. M.; Unruh, D. K.; Bosch, E.; Bowling, N. P.; Cozzolino, A. F. Triple-Pnictogen Bonding as a Tool for Supramolecular Assembly. *Inorg. Chem.* **2019**, *58*, 16227−16235.

(8) Werz, D. B.; Gleiter, R.; Rominger, F. Nanotube Formation Favored by Chalcogen−Chalcogen Interactions. *J. Am. Chem. Soc.* **2002**, *124*, 10638−10639.

(9) Pascoe, D. J.; Ling, K. B.; Cockroft, S. L. The Origin of Chalcogen-Bonding Interactions. *J. Am. Chem. Soc.* **2017**, *139*, 15160−15167.

(10) Gleiter, R.; Haberhauer, G.; Werz, D. B.; Rominger, F.; Bleiholder, C. From Noncovalent Chalcogen−Chalcogen Interactions to Supramolecular Aggregates: Experiments and Calculations. *Chem. Rev.* **2018**, *118*, 2010−2041.

(11) Haberhauer, G.; Gleiter, R. The Nature of Strong Chalcogen Bonds Involving Chalcogen-Containing Heterocycles. *Angew. Chem., Int. Ed.* **2020**, *59*, 21236−21243.

(12) Bauzá, A.; Frontera, A. Aerogen Bonding Interaction: A New Supramolecular Force? *Angew. Chem., Int. Ed.* **2015**, *54*, 7340−7343.

(13) Mallada, B.; Gallardo, A.; Lamanec, M.; De La Torre, B.; Špirko, V.; Hobza, P.; Jelinek, P. Real-Space Imaging of Anisotropic Charge of σ-Hole by Means of Kelvin Probe Force Microscopy. *Science* **2021**, *374*, 863−867.

(14) Scilabra, P.; Terraneo, G.; Resnati, G. The Chalcogen Bond in Crystalline Solids: A World Parallel to Halogen Bond. *Acc. Chem. Res.* **2019**, *52*, 1313−1324.

(15) Aakeroy, C. B.; Bryce, D. L.; Desiraju, G. R.; Frontera, A.; Legon, A. C.; Nicotra, F.; Rissanen, K.; Scheiner, S.; Terraneo, G.; Metrangolo, P.; Resnati, G. Definition of the Chalcogen Bond (IUPAC Recommendations 2019). *Pure Appl. Chem.* **2019**, *91*, 1889−1892.

(16) Schwerdtfeger, P.; Nagle, J. K. 2018 Table of Static Dipole Polarizabilities of the Neutral Elements in the Periodic Table. *Mol. Phys.* **2019**, *117*, 1200−1225.

(17) Nayak, S. K.; Kumar, V.; Murray, J. S.; Politzer, P.; Terraneo, G.; Pilati, T.; Metrangolo, P.; Resnati, G. Fluorination Promotes

Chalcogen Bonding in Crystalline Solids. *CrystEngComm* **2017**, *19*, 4955−4959.
(18) Ho, P. C.; Szydlowski, P.; Sinclair, J.; Elder, P. J. W.; Kübel, J.; Gendy, C.; Lee, L. M.; Jenkins, H.; Britten, J. F.; Morim, D. R.; Vargas-Baca, I. Supramolecular Macrocycles Reversibly Assembled by Te...O Chalcogen Bonding. *Nat. Commun.* **2016**, *7*, 11299.
(19) Kremer, A.; Fermi, A.; Biot, N.; Wouters, J.; Bonifazi, D. Supramolecular Wiring of Benzo-1,3-chalcogenazoles through Programmed Chalcogen Bonding Interactions. *Chem. Eur. J.* **2016**, *22*, 5665−5675.
(20) Carugo, O.; Resnati, G.; Metrangolo, P. Chalcogen Bonds Involving Selenium in Protein Structures. *ACS Chem. Biol.* **2021**, *16*, 1622−1627.
(21) Shi, D.; Cao, J.; Weng, P.; Yan, X.; Li, Z.; Jiang, Y.-B. Chalcogen Bonding Mediates the Formation of Supramolecular Helices of Azapeptides in Crystals. *Org. Biomol. Chem.* **2021**, *19*, 6397−6401.
(22) Kumar, V.; Xu, Y.; Bryce, D. L. Double Chalcogen Bonds: Crystal Engineering Stratagems via Diffraction and Multinuclear Solid-State Magnetic Resonance Spectroscopy. *Chem. Eur. J.* **2020**, *26*, 3275−3286.
(23) Huynh, H.-T.; Jeannin, O.; Fourmigué, M. Organic Selenocyanates as Strong and Directional Chalcogen Bond Donors For Crystal Engineering. *Chem. Commun.* **2017**, *53*, 8467−8469.
(24) Xu, Y.; Kumar, V.; Bradshaw, M. J. Z.; Bryce, D. L. Chalcogen-Bonded Cocrystals of Substituted Pyridine N-Oxides and Chalcogenodiazoles: An X-ray Diffraction and Solid-State NMR Investigation. *Cryst. Growth Des.* **2020**, *20*, 7910−7920.
(25) Kumar, V.; Leroy, C.; Bryce, D. L. Halide Ion Recognition via Chalcogen Bonding in the Solid State and in Solution. Directionality and Linearity. *CrystEngComm* **2018**, *20*, 6406−6411.
(26) Benz, S.; Macchione, M.; Verolet, Q.; Mareda, J.; Sakai, N.; Matile, S. Anion Transport with Chalcogen Bonds. *J. Am. Chem. Soc.* **2016**, *138*, 9093−9096.
(27) Mahmudov, K. T.; Kopylovich, M. N.; Guedes da Silva, M. F. C.; Pombeiro, A. J. L. Chalcogen Bonding in Synthesis, Catalysis and Design of Materials. *Dalton Trans.* **2017**, *46*, 10121−10138.
(28) Wonner, P.; Vogel, L.; Düser, M.; Gomes, L.; Kniep, F.; Mallick, B.; Werz, D. B.; Huber, S. M. Carbon−Halogen Bond Activation by Selenium-Based Chalcogen Bonding. *Angew. Chem., Int. Ed.* **2017**, *56*, 12009−12012.
(29) Thomas, S. P.; Kumar, V.; Alhameedi, K.; Guru Row, T. N. Non-Classical Synthons: Supramolecular Recognition by S···O Chalcogen Bonding in Molecular Complexes of Riluzole. *Chem. Eur. J.* **2019**, *25*, 3591−3597.
(30) Thomas, S. P.; Satheeshkumar, K.; Mugesh, G.; Guru Row, T. N. Unusually Short Chalcogen Bonds Involving Organoselenium: Insights into the Se−N Bond Cleavage Mechanism of the Antioxidant Ebselen and Analogues. *Chem. Eur. J.* **2015**, *21*, 6793−6800.
(31) Clark, T.; Hennemann, M.; Murray, J. S.; Politzer, P. Halogen Bonding: the σ-Hole. *J. Mol. Model.* **2007**, *13*, 291−296.
(32) Brezgunova, M. E.; Lieffrig, J.; Aubert, E.; Dahaoui, S.; Fertey, P.; Lebègue, S.; Ángyan, J. G.; Fourmigué, M.; Espinosa, E. Chalcogen Bonding: Experimental and Theoretical Determinations from Electron Density Analysis. Geometrical Preferences Driven by Electrophilic−Nucleophilic Interactions. *Cryst. Growth Des.* **2013**, *13*, 3283−3289.
(33) Politzer, P.; Murray, J. S.; Clark, T.; Resnati, G. The σ-Hole Revisited. *Phys. Chem. Chem. Phys.* **2017**, *19*, 32166−32178.
(34) Klapötke, T. M.; Krumm, B.; Scherr, M. Homoleptic Selenium Cyanides: Attempted Preparation of Se(CN)4 and Redetermination of the Crystal Structure of Se(CN)2. *Inorg. Chem.* **2008**, *47*, 7025−7028.
(35) Klapötke, T. M.; Krumm, B.; Gálvez-Ruiz, J. C.; Nöth, H.; Schwab, I. Experimental and Theoretical Studies of Homoleptic Tellurium CyanidesTe(CN)x: Crystal Structure of Te(CN)2. *Eur. J. Inorg. Chem.* **2004**, *2004*, 4764−4769.
(36) Cozzolino, A. F.; Whitfield, P. S.; Vargas-Baca, I. Supramolecular Chromotropism of the Crystalline Phases of 4,5,6,7-Tetrafluorobenzo-2,1,3-telluradiazole. *J. Am. Chem. Soc.* **2010**, *132*, 17265−17270.
(37) Ho, P. C.; Lomax, J.; Tomassetti, V.; Britten, J. F.; Vargas-Baca, I. Competing Effects of Chlorination on the Strength of Te···O Chalcogen Bonds Select the Structure of Mixed Supramolecular Macrocyclic Aggregates of Iso-Tellurazole N-Oxides. *Chem. Eur. J.* **2021**, *27*, 10849−10853.
(38) Semenov, N. A.; Lonchakov, A. V.; Pushkarevsky, N. A.; Suturina, E. A.; Korolev, V. V.; Lork, E.; Vasiliev, V. G.; Konchenko, S. N.; Beckmann, J.; Gritsan, N. P.; Zibarev, A. V. Coordination of Halide and Chalcogenolate Anions to Heavier 1,2,5-Chalcogenadiazoles: Experiment and Theory. *Organometallics* **2014**, *33*, 4302−4314.
(39) Garrett, G. E.; Gibson, G. L.; Straus, R. N.; Seferos, D. S.; Taylor, M. S. Chalcogen Bonding in Solution: Interactions of Benzotelluradiazoles with Anionic and Uncharged Lewis Bases. *J. Am. Chem. Soc.* **2015**, *137*, 4126−4133.
(40) Benz, S.; Lopez-Andarias, J.; Mareda, J.; Sakai, N.; Matile, S. Catalysis with Chalcogen Bonds. *Angew. Chem., Int. Ed.* **2017**, *56*, 812−815.
(41) Navarro-Garcia, E.; Galmes, B.; Velasco, M. D.; Frontera, A.; Caballero, A. Anion Recognition by Neutral Chalcogen Bonding Receptors: Experimental and Theoretical Investigations. *Chem. Eur. J.* **2020**, *26*, 4706−4713.
(42) Cozzolino, A. F.; Elder, P. J. W.; Vargas-Baca, I. A Survey of Tellurium-Centered Secondary-Bonding Supramolecular Synthons. *Coord. Chem. Rev.* **2011**, *255*, 1426−1438.
(43) Biot, N.; Bonifazi, D. Programming Recognition Arrays through Double Chalcogen-Bonding Interactions. *Chem. Eur. J.* **2018**, *24*, 5439−5443.
(44) Jeannin, O.; Huynh, H.-T.; Riel, A. M. S.; Fourmigué, M. Chalcogen Bonding Interactions in Organic Selenocyanates: From Cooperativity to Chelation. *New J. Chem.* **2018**, *42*, 10502−10509.
(45) Riel, A. M. S.; Huynh, H.-T.; Jeannin, O.; Berryman, O.; Fourmigué, M. Organic Selenocyanates as Halide Receptors: From Chelation to One-Dimensional Systems. *Cryst. Growth Des.* **2019**, *19*, 1418−1425.
(46) Riel, A. M. S.; Jeannin, O.; Berryman, O. B.; Fourmigué, M. Co-crystals of an Organic Triselenocyanate with Ditopic Lewis Bases: Recurrent Chalcogen Bond Interactions Motifs. *Acta Crystallogr.* **2019**, *B75*, 34−38.
(47) Huynh, H.-T.; Jeannin, O.; Aubert, E.; Espinosa, E.; Fourmigué, M. Chalcogen Bonding Interactions in Chelating, Chiral Bis(Selenocyanates). *New J. Chem.* **2021**, *45*, 76−84.
(48) Sen, S.; Kaseman, D. C.; Hung, I.; Gan, Z. ^{77}Se Nuclear Spin−Lattice Relaxation in Binary Ge−Se Glasses: Insights into Floppy Versus Rigid Behavior of Structural Units. *J. Phys. Chem. B* **2015**, *119*, 5747−5753.
(49) Kumar, V.; Xu, Y.; Leroy, C.; Bryce, D. L. Direct Investigation of Chalcogen Bonds by Multinuclear Solid-State Magnetic Resonance and Vibrational Spectroscopy. *Phys. Chem. Chem. Phys.* **2020**, *22*, 3817−3824.
(50) Lari, A.; Gleiter, R.; Rominger, F. Supramolecular Organization Based on van der Waals Forces: Syntheses and Solid State Structures of Isomeric [6.6]Cyclophanes with 2,5-Diselenahex-3-yne Bridges. *Eur. J. Org. Chem.* **2009**, *2009*, 2267−2274.
(51) Hojjatie, M.; Muralidharan, S.; Freiser, H. Synthesis and Multinuclear NMR Characterizations of Some [3.3]Diselena- And [4.4]Tetraselenacyclophanes. *Tetrahedron* **1989**, *45*, 1611−1622.
(52) Truong, K.-N.; Rautiainen, J. M.; Rissanen, K.; Puttreddy, R. The C−I···$^{-}$O−N^{+} Halogen Bonds with Tetraiodoethylene and Aromatic N-Oxides. *Cryst. Growth Des.* **2020**, *20*, 5330−5337.
(53) Kumar, V.; Pilati, T.; Terraneo, G.; Meyer, F.; Metrangolo, P.; Resnati, G. Halogen Bonded Borromean Networks by Design: Topology Invariance and Metric Tuning in a Library of Multi-Component Systems. *Chem. Sci.* **2017**, *8*, 1801−1810.
(54) Gale, P. A.; Gunnlaugsson, T. Preface: Supramolecular Chemistry of Anionic Species Themed Issue. *Chem. Soc. Rev.* **2010**, *39*, 3595−3596.

https://doi.org/10.1021/acsorginorgau.1c00051
ACS Org. Inorg. Au 2022, 2, 252−260

(55) Saha, S.; Desiraju, G. R. Acid···Amide Supramolecular Synthon in Cocrystals: From Spectroscopic Detection to Property Engineering. *J. Am. Chem. Soc.* **2018**, *140*, 6361−6373.
(56) Vasylyeva, V.; Catalano, C.; Nervi, C.; Gobetto, R.; Metrangolo, P.; Resnati, G. Characteristic Redshift and Intensity Enhancement as Far-IR Fingerprints of the Halogen Bond Involving Aromatic Donors. *CrystEngComm* **2016**, *18*, 2247−2250.
(57) Herzfeld, J.; Berger, A. E. Sideband Intensities in NMR Spectra of Samples Spinning at the Magic Angle. *J. Chem. Phys.* **1980**, *73*, 6021−6030.
(58) Massiot, D.; Fayon, F.; Capron, M.; King, I.; Le Calvé, S.; Alonso, B.; Durand, J. O.; Bujoli, B.; Gan, Z.; Hoatson, G. Modelling One- and Two-Dimensional Solid-State NMR Spectra. *Magn. Reson. Chem.* **2002**, *40*, 70−76.

https://doi.org/10.1021/acsorginorgau.1c00051
ACS Org. Inorg. Au 2022, 2, 252−260